Smart Structures and Systems, *Vol. 14, No. 2 (2014) 247-266*
DOI: http://dx.doi.org/10.12989/sss.2014.14.2.247

Modeling and performance evaluation of a piezoelectric energy harvester with segmented electrodes

Hongyan Wang*[1,2], Lihua Tang[3,4], Xiaobiao Shan[1], Tao Xie[1] and Yaowen Yang[3]

[1]*State Key Laboratory of Robotics and System, Harbin Institute of Technology, No.2 Yikuang Street, Nangang District, Harbin, Heilongjiang, China*
[2]*College of Computer and Control Engineering, Qiqihar University, No.42 Wenhua Street, Qiqihar, Heilongjiang, China*
[3]*School of Civil and Environmental Engineering, Nanyang Technological University, 50 Nanyang Avenue, Singapore 639798*
[4]*Department of Mechanical Engineering, University of Auckland, 20 Symonds Street, Auckland 1010, New Zealand*

(Received December 13, 2012, Revised January 27, 2014, Accepted February 11, 2014)

Abstract. Conventional cantilevered piezoelectric energy harvesters (PEHs) are usually fabricated with continuous electrode configuration (CEC), which suffers from the electrical cancellation at higher vibration modes. Though previous research pointed out that the segmented electrode configuration (SEC) can address this issue, a comprehensive evaluation of the PEH with SEC has yet been reported. With the consideration of delivering power to a common load, the AC outputs from all segmented electrode pairs should be rectified to DC outputs separately. In such case, theoretical formulation for power estimation becomes challenging. This paper proposes a method based on equivalent circuit model (ECM) and circuit simulation to evaluate the performance of the PEH with SEC. First, the parameters of the multi-mode ECM are identified from theoretical analysis. The ECM is then established in SPICE software and validated by the theoretical model and finite element method (FEM) with resistive loads. Subsequently, the optimal performances with SEC and CEC are compared considering the practical DC interface circuit. A comprehensive evaluation of the advantageous performance with SEC is provided for the first time. The results demonstrate the feasibility of using SEC as a simple and effective means to improve the performance of a cantilevered PEH at a higher mode.

Keywords: piezoelectric cantilever; energy harvesting; segmented electrode configuration; equivalent circuit model; circuit simulation

1. Introduction

In recent years, a variety of wireless sensing electronics have emerged and provided some new applications for structural and environmental monitoring. However, the batteries used to power wireless sensing electronics bring some disadvantages, such as large size, limited lifespan, and costly replacement (Paradiso and Starner 2005, Mathuna *et al*. 2008). Vibration energy harvesting provides a promising solution and has attracted immense research interests owing to its potential to

*Corresponding author, Ph. D., E-mail: wanghongyan1993@163.com

http://www.techno-press.org/?journal=sss&subpage=8 ISSN: 1738-1584 (Print), 1738-1991 (Online)

implement low-cost self-powered wireless sensors. The abundant vibration energy in the environment can be converted to useful electricity via piezoelectric (Anton and Sodano 2007, Yang *et al*. 2009, Guan *et al*. 2012, Zhang and Zhu 2012, Aladwani *et al*. 2012, Wang *et al*. 2012, Wu *et al*. 2012), electromagnetic (Jung *et al.* 2011, Foisal *et al.* 2012) or electrostatic transductions (Roundy *et al*. 2003, Lallart *et al*. 2011). Piezoelectric transduction is widely pursued due to the high power density and ease for application as compared to the other two transductions. Therefore, piezoelectric transduction is more suitable for small-scale systems (Beeby *et al.* 2006, Liu *et al*. 2011, Tang *et al*. 2012).

Conventional unimorph/bimorph piezoelectric energy harvesters (PEH) are usually fabricated with continuous electrode configuration (CEC). The energy harvester with CEC can only work around the first resonance efficiently due to the cancellation of the electrical output around higher modes. To improve the power output at higher modes, two approaches have been resorted to in the reported literature. One approach is to change the direction of polarization of the piezoelectric plate in different region to avoid the electrical cancellation (Kim *et al*. 2005). Another approach is to use the segmented electrode configuration (SEC) by creating discontinuity at the strain node of the PEH and switching the leads of the segmented electrodes or connecting multi-rectifiers to avoid the electrical cancellation (Erturk *et al*. 2009). The SEC approach is more flexible compared to the patterned poling process in the vibration-based energy harvesting since the latter requires re-fabrication of the PEH if the vibration modes change. Multi-rectifiers are often used since no effort is required to switch the leads of the segmented electrodes for different vibration modes.

The efficient design of a PEH requires accurate modeling of its behavior so as to quickly evaluate the system performance. A single-degree-of-freedom (SDOF) model is available in some early energy harvesting literature (Roundy *et al*. 2003, du Toit *et al*. 2005), which can predict the power output by approximating an energy harvesting structure as a spring+mass+damper+piezo system. However, the SDOF model can only provide preliminary insights into piezoelectric energy harvesting as it lacks the information of accurate strain distribution and higher vibration modes of an energy harvesting structure. An improved modeling approach based on the Rayleigh-Ritz formulation can provide a discrete model of the distributed parameter system. Hagood *et al*. (1990) provided a good starting point to model a piezoelectric actuator/sensor using the Rayleigh-Ritz formulation. Following this work, Sodano *et al*. (2004) and du Toit *et al*. (2005) established approximate distributed parameter models for a cantilevered PEH based on the Euler–Bernoulli beam theory. Furthermore, Erturk and Inman (2008b) presented a close-form analytical solution of a cantilevered PEH using the summation of modal responses. However, in the above analytical models, the estimation of power output is achieved by simplifying the energy harvesting interface circuit as a pure resistor. Theoretical formulation becomes challenging when practical interface circuits are considered, which include nonlinear electrical components such as rectifiers.

Some researchers have developed the equivalent circuit model (ECM) of piezoelectric energy harvesters. The parameters in ECM can be obtained using theoretical approach or finite element method (Elvin and Elvin 2009, Yang and Tang 2009, Tang and Yang 2012). With the established ECM, circuit simulation using the SPICE software can be utilized to predict the performance of PEH with sophisticated interface circuits such as the Synchronized Switching Harvesting on Inductor (SSHI) technique (Guyomar *et al*. 2005, Liang and Liao 2011, 2012, Lien *et al*. 2010, 2011) and the Synchronized Charge Extraction (SCE) technique (Tang and Yang 2011). However, the previous studies focused on the ECM of the PEH with CEC, where the PEH only has a single electrical output port.

Unlike the previous efforts on ECM, in this paper, we establish a multi-mode ECM of the cantilevered PEH with SEC, where the PEH have two electrical output ports. The parameters used in the ECM are identified from the theoretical analysis. A numerical example is presented to validate the derived ECM of the PEH with SEC by considering pure resistors. Subsequently, with the validated ECM, the performance of the PEH with SEC is studied to illustrate the feasibility of using SEC as a simple and effective means to enhance the power output at a higher resonance frequency.

2. Theoretical modeling

Figs. 1(a) and 1(b) show a cantilevered PEH with CEC and SEC, respectively. The bimorph PEH consists of two piezoelectric layers (PZT_1 and PZT_2) and one substrate metallic layer. A proof mass is attached to the free end of the piezoelectric cantilever. In Fig. 1(a), the bimorph layers are oppositely polarized in the z-direction and connected in series. The output terminal is directly connected to a resistor R_L. Using the etching method, a continuous electrode pair can be partitioned into multiple electrode pairs. In this paper, the focus is the performance of the cantilevered PEH with the SEC at the second bending mode. Hence, the discontinuity of the electrode is located at the location of the strain node for the second bending mode. After the electrode pair is segmented, one electrical output of the conventional piezoelectric cantilever is separated into two electrical outputs. In Fig. 1(b), the segmented electrode at the left of the strain node is defined as SEC1 and the other at the right is defined as SEC2. The two output terminals of SEC1 and SEC2 are connected to the resistors R_{L1} and R_{L2}, respectively.

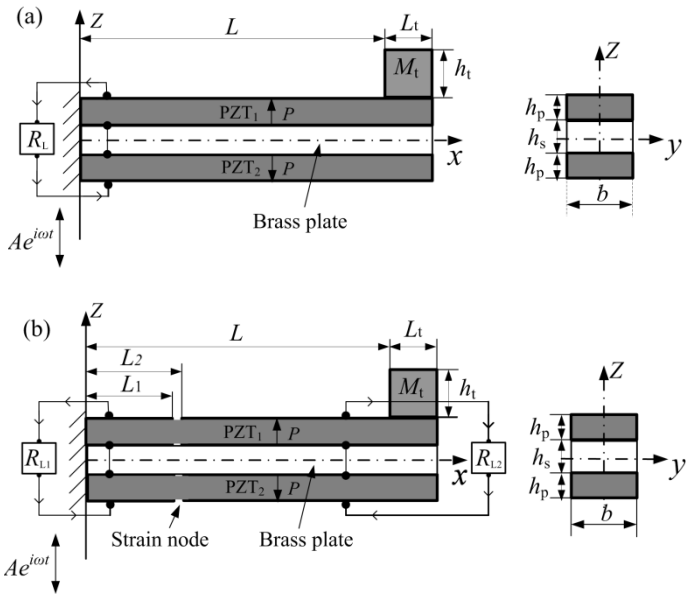

Fig. 1 Cantilevered PEH with (a) CEC and (b) SEC

The theoretical model of the cantilevered PEH with SEC is derived by using the energy approach. The following assumptions are used in formulation: (a) the piezoelectric cantilever is considered as an Euler-Bernoulli beam; (b) the overhang mass including the proof mass and the outer portion of the piezoelectric beam (from L to $L+L_t$) is considered as rigid and contains rotational terms; (c) the strain rate damping and viscous air damping are proportional to the bending stiffness and mass per length of the beam, respectively; (d) the electric field is uniform through the thickness in the piezoelectric layers.

2.1 Kinetic energy

Besides the translational motion caused by the bending of the beam, according to assumption (b), the overhang mass at the junction $x=L$ is allowed to rotate. Hence, the kinetic energy K of the energy harvesting system include the translational and rotational kinetic energies from the piezoelectric beam and the overhang mass, which is given as

$$K = \frac{1}{2}\int_{V_s} \rho_s \dot{w}^2 dV_s + \frac{1}{2}\int_{V_p} \rho_p \dot{w}^2 dV_p + \frac{1}{2} M_0 \left[\dot{w}(L)\right]^2 + S_0 \dot{w}(L)\dot{w}'(L) + \frac{1}{2} I_0 \left[\dot{w}'(L)\right]^2 \tag{1}$$

where $(\cdot)=\partial/\partial t$; $(')=\partial/\partial x$; V and ρ stand for volume and density, respectively; the subscripts s and p stand for the substrate material and the piezoelectric material, respectively; w is the beam displacement relative to the base; L is the active length of piezoelectric beam; and M_0, S_0 and I_0 are the mass, the static moment and the inertia moment about the junction $x=L$ of the overhang (including proof mass and the outer portion of the piezoelectric beam), respectively.

Using the Raleigh-Ritz method, the displacement of the piezoelectric beam can be written as

$$w = w(x,t) = \sum_{i=1}^{n} \psi_i(x) r_i(t) = \boldsymbol{\psi}(x)\mathbf{r}(t) = \boldsymbol{\psi}\mathbf{r} \tag{2}$$

where $\psi_i(x)$ and $r_i(t)$ are the mode shape and the modal coordinate of the i-th mode, respectively; and n is the number of considered modes. The bending mode shape of a clamped-free beam with a proof mass is given as (du Toit *et al*. 2005, Kim *et al*. 2010)

$$\psi_i(x) = c[(\cosh\alpha_i x - \cos\alpha_i x) - \frac{A_{12}}{A_{11}}(\sinh\alpha_i x - \sin\alpha_i x)] \tag{3}$$

where the mode shape is normalized to $\psi_i(L)=2$, which gives $c = 2/[(\cosh\alpha_i L - \cos\alpha_i L) - (A_{12}/A_{11})(\sinh\alpha_i L - \sin\alpha_i L)]$; α_i is the eigenvalue of the i-th mode, which can be solved according to the determinant $\begin{vmatrix} A_{11} & A_{12} \\ A_{21} & A_{22} \end{vmatrix} = 0$, where

$$\begin{cases} A_{11} = (\sinh\bar{\alpha}_i + \sin\bar{\alpha}_i) + \bar{\alpha}_i^3 \bar{I}_0 (-\cosh\bar{\alpha}_i + \cos\bar{\alpha}_i) + \bar{\alpha}_i^2 \bar{S}_0 (-\sinh\bar{\alpha}_i + \sin\bar{\alpha}_i) \\ A_{12} = (\cosh\bar{\alpha}_i + \cos\bar{\alpha}_i) + \bar{\alpha}_i^3 \bar{I}_0 (-\sinh\bar{\alpha}_i - \sin\bar{\alpha}_i) + \bar{\alpha}_i^2 \bar{S}_0 (-\cosh\bar{\alpha}_i + \cos\bar{\alpha}_i) \\ A_{21} = (\cosh\bar{\alpha}_i + \cos\bar{\alpha}_i) + \bar{\alpha}_i \bar{M}_0 (\sinh\bar{\alpha}_i - \sin\bar{\alpha}_i) + \bar{\alpha}_i^2 \bar{S}_0 (\cosh\bar{\alpha}_i - \cos\bar{\alpha}_i) \\ A_{22} = (\sinh\bar{\alpha}_i - \sin\bar{\alpha}_i) + \bar{\alpha}_i \bar{M}_0 (\cosh\bar{\alpha}_i - \cos\bar{\alpha}_i) + \bar{\alpha}_i^2 \bar{S}_0 (\sinh\bar{\alpha}_i + \sin\bar{\alpha}_i) \end{cases} \tag{4}$$

where the dimensionless terms are given as

$$\bar{\alpha}_i=\alpha_i L\,,\ \ \bar{M}_0=M_0/((m_\mathrm{s}+m_\mathrm{p})L)\,,\ \ \bar{S}_0=S_0/((m_\mathrm{s}+m_\mathrm{p})L^2)\,,\ \ \bar{I}_0=I_0/((m_\mathrm{s}+m_\mathrm{p})L^3) \tag{5}$$

where m_s is the mass per length of the substrate layer, $m_\mathrm{s}=\rho_\mathrm{s}h_\mathrm{s}b$; m_p are the mass per length of the piezoelectric layers, $m_\mathrm{p}=2\rho_\mathrm{p}h_\mathrm{p}b$; h_s and h_p are the thickness of the substrate layer and a piezoelectric layer, respectively; b is the width of the piezoelectric beam; and M_0, S_0 and I_0 can be expressed as

$$\begin{cases} M_0=m_\mathrm{t}L_\mathrm{t}+(m_\mathrm{s}+m_\mathrm{p})L_\mathrm{t} \\ S_0=M_0L_\mathrm{t}/2 \\ I_0=m_\mathrm{t}L_\mathrm{t}(L_\mathrm{t}^2+h_\mathrm{t}^2)/3+(m_\mathrm{s}+m_\mathrm{p})L_\mathrm{t}[L_\mathrm{t}^2+(h_\mathrm{s}+2h_\mathrm{p})^2]/3 \end{cases} \tag{6}$$

where m_t is the mass per length of the proof mass, $m_\mathrm{t}=\rho_\mathrm{t}h_\mathrm{t}b$, where ρ_t and h_t are the volume density and the thickness of the proof mass, respectively; and L_t is the length of the proof mass.

Submitting Eq. (2) into Eq. (1) and integrating in the y- and z- directions, the kinetic energy of the PEH is reduced to

$$K=\frac{1}{2}\int_0^L(m_\mathrm{s}+m_\mathrm{p})\left(\boldsymbol{\psi}\dot{\mathbf{r}}\right)^2dx+\frac{1}{2}M_0\left(\boldsymbol{\psi}(L)\dot{\mathbf{r}}\right)^2+S_0\boldsymbol{\psi}(L)\boldsymbol{\psi}'(L)\dot{\mathbf{r}}^2+\frac{1}{2}I_0\left(\boldsymbol{\psi}'(L)\dot{\mathbf{r}}\right)^2 \tag{7}$$

2.2 Internal potential energy

The internal potential energy of the PEH is defined as

$$U=\frac{1}{2}\int_{V_\mathrm{s}}S_\mathrm{s}T_\mathrm{s}dV_\mathrm{s}+\frac{1}{2}\int_{V_\mathrm{p}}S_\mathrm{p}T_\mathrm{p}dV_\mathrm{p} \tag{8}$$

where T is the stress and S is the strain. Based on assumption (a), the axial strain $S(x, t)$ can be expressed as

$$S(x,t)=-\hat{z}\frac{\partial^2w(x,t)}{\partial x^2}=-\hat{z}w'' \tag{9}$$

where $\hat{z}$ is the position from the neutral axis of the piezoelectric beam.

According to the constitutive equations for the substrate layer and piezoelectric layer, the stress in the piezoelectric beam can be written as

$$T_\mathrm{s}=c_\mathrm{s}S_\mathrm{s} \tag{10}$$

$$T_\mathrm{p}=c_{11}^\mathrm{E}S_\mathrm{p}-e_{31}E \tag{11}$$

where c_s is the stiffness of the substrate material; c_{11}^E is the stiffness of the piezoelectric material at constant electric field; e_{31} is the piezoelectric constant; and E is the electric field. Based on assumption (d), the electric field of the PEH with SEC1 and SEC2 is expressed as:

$$E=\begin{cases}\dfrac{\mathrm{V}_{\mathrm{R}1}}{2h_{\mathrm{p}}}, & 0\le x\le L_1\\ 0, & L_1\le x\le L_2\\ \dfrac{\mathrm{V}_{\mathrm{R}2}}{2h_{\mathrm{p}}}, & L_2\le x\le L+L_{\mathrm{t}}\end{cases} \tag{12}$$

Submitting Eqs. (10) and (11) into Eq. (8), the potential energy is written as

$$U=\frac{1}{2}\int_{V_{\mathrm{s}}}S_{\mathrm{s}}c_{\mathrm{s}}S_{\mathrm{s}}dV_{\mathrm{s}}+\frac{1}{2}\int_{V_{\mathrm{p}}}S_{\mathrm{p}}c_{11}^{\mathrm{E}}S_{\mathrm{p}}dV_{\mathrm{p}}-\frac{1}{2}\int_{V_{\mathrm{p}}}S_{\mathrm{p}}e_{31}EdV_{\mathrm{p}}=U_{\mathrm{s}}+U_{\mathrm{ps}}-U_{\mathrm{pe}} \tag{13}$$

where the first two terms, U_{s} and U_{ps}, are only dependent on the strain; the last term, U_{pe}, is dependent on both the strain and the electric field. Submitting Eqs. (2), (9) and (12) into Eq. (13) and integrating in the y- direction, the sum of U_{s} and U_{ps} is given by

$$\begin{aligned}U_{\mathrm{s}}+U_{\mathrm{ps}}=&\frac{1}{2}\int_0^L\int_{-h_{\mathrm{s}}/2}^{h_{\mathrm{s}}/2}c_{\mathrm{s}}\hat{z}^2\left(\boldsymbol{\psi}''\mathbf{r}\right)^2bd\hat{z}dx\\&+\frac{1}{2}\int_0^L\int_{-h_{\mathrm{s}}/2-h_{\mathrm{p}}}^{-h_{\mathrm{s}}/2}c_{11}^{\mathrm{E}}\hat{z}^2\left(\boldsymbol{\psi}''\mathbf{r}\right)^2bd\hat{z}dx+\frac{1}{2}\int_0^L\int_{h_{\mathrm{s}}/2}^{h_{\mathrm{s}}/2+h_{\mathrm{p}}}c_{11}^{\mathrm{E}}\hat{z}^2\left(\boldsymbol{\psi}''\mathbf{r}\right)^2bd\hat{z}dx\end{aligned} \tag{14}$$

The term, U_{pe}, is given by

$$\begin{aligned}U_{\mathrm{pe}}=&\frac{1}{2}\int_0^L\int_{-h_{\mathrm{s}}/2-h_{\mathrm{p}}}^{-h_{\mathrm{s}}/2}\hat{z}\boldsymbol{\psi}''\mathbf{r}e_{31}\frac{\mathrm{V}_{\mathrm{R1}}}{2h_{\mathrm{p}}}bd\hat{z}dx+\frac{1}{2}\int_0^L\int_{h_{\mathrm{s}}/2}^{h_{\mathrm{s}}/2+h_{\mathrm{p}}}\left(-\hat{z}\right)\boldsymbol{\psi}''\mathbf{r}e_{31}\frac{\mathrm{V}_{\mathrm{R1}}}{2h_{\mathrm{p}}}bd\hat{z}dx\\&+\frac{1}{2}\int_{L_2}^L\int_{-h_{\mathrm{s}}/2-h_{\mathrm{p}}}^{-h_{\mathrm{s}}/2}\hat{z}\boldsymbol{\psi}''\mathbf{r}e_{31}\frac{\mathrm{V}_{\mathrm{R2}}}{2h_{\mathrm{p}}}bd\hat{z}dx+\frac{1}{2}\int_{L_2}^L\int_{h_{\mathrm{s}}/2}^{h_{\mathrm{s}}/2+h_{\mathrm{p}}}\left(-\hat{z}\right)\boldsymbol{\psi}''\mathbf{r}e_{31}\frac{\mathrm{V}_{\mathrm{R2}}}{2h_{\mathrm{p}}}bd\hat{z}dx\end{aligned} \tag{15}$$

Eq. (15) can be reduced through integrating with respect to $\hat{z}$ and then rearranged by relating the voltage and current $\mathrm{V}_{\mathrm{R1}}=R_{\mathrm{L1}}\dot{q}_{\mathrm{R1}}$, $\mathrm{V}_{\mathrm{R2}}=R_{\mathrm{L2}}\dot{q}_{\mathrm{R2}}$ as follows

$$\begin{aligned}U_{\mathrm{pe}}=&-\frac{h_{\mathrm{s}}+h_{\mathrm{p}}}{4}\int_0^{L_1}\boldsymbol{\psi}''\mathbf{r}e_{31}\mathrm{V}_{\mathrm{R1}}bdx-\frac{h_{\mathrm{s}}+h_{\mathrm{p}}}{4}\int_{L_2}^L\boldsymbol{\psi}''\mathbf{r}e_{31}\mathrm{V}_{\mathrm{R2}}bdx\\=&-\frac{h_{\mathrm{pc}}e_{31}b}{2}\left(\int_0^{L_1}\boldsymbol{\psi}''\mathbf{r}R_{\mathrm{L1}}\dot{q}_{\mathrm{R1}}dx+\int_{L_2}^L\boldsymbol{\psi}''\mathbf{r}R_{\mathrm{L2}}\dot{q}_{\mathrm{R2}}bdx\right)\end{aligned} \tag{16}$$

where h_{pc} is the distance from the centre of piezoelectric layer to the neutral axis, $h_{\mathrm{pc}}=(h_{\mathrm{s}}+h_{\mathrm{p}})/2$.

2.3 Electrical energy

The electrical energy of the PEH is defined as

$$W_{\mathrm{e}}=\frac{1}{2}\int_{V_{\mathrm{p}}}EDdV_{\mathrm{p}} \tag{17}$$

where D is the electrical displacement.

The electrical displacement can be calculated according to the constitutive equation for the piezoelectric layer as

$$D = e_{31} S_{\mathrm{p}} + \varepsilon_{33}^{\mathrm{S}} E \tag{18}$$

where e_{31} is the piezoelectric constant; and $\varepsilon_{33}^{\mathrm{S}}$ is the dielectric constant of the piezoelectric material at constant strain.

Submitting Eq. (18) into Eq. (17), the electrical potential energy is written as

$$\begin{aligned} W_{\mathrm{e}} &= \frac{1}{2}\int_{V_{\mathrm{p}}} E e_{31} S_{\mathrm{p}} dV_{\mathrm{p}} + \frac{1}{2}\int_{V_{\mathrm{p}}} E \varepsilon_{33}^{\mathrm{S}} E dV_{\mathrm{p}} \\ &= W_{\mathrm{pe1}} + W_{\mathrm{pe2}} \end{aligned} \tag{19}$$

where the first term, W_{pe1}, is dependent on the electric field and the strain; the second term, W_{pe2}, is dependent on the electric field but independent of the strain. Submitting Eqs. (2) and (12) into Eq. (19), integrating in the y- and z- directions and rearranging the equation by relating the voltage to current, we obtain

$$W_{\mathrm{pe1}} = -\frac{h_{\mathrm{pc}} e_{31} b}{2}\left(\int_0^{L_1} \boldsymbol{\psi}'' \mathbf{r} R_{\mathrm{L1}} \dot{q}_{\mathrm{R1}} dx + \int_{L_2}^{L} \boldsymbol{\psi}'' \mathbf{r} R_{\mathrm{L2}} \dot{q}_{\mathrm{R2}} b dx\right) \tag{20}$$

and

$$\begin{aligned} W_{\mathrm{pe2}} &= \frac{1}{4h_{\mathrm{p}}}\int_0^{L_1} \varepsilon_{33}^{S} b \mathrm{V}_{\mathrm{R1}}{}^2 dx + \frac{1}{4h_{\mathrm{p}}}\int_{L_2}^{L+L_1} \varepsilon_{33}^{S} b \mathrm{V}_{\mathrm{R2}}{}^2 dx \\ &= \frac{\varepsilon_{33}^{S} b}{4h_{\mathrm{p}}}\left(\int_0^{L_1} \left(R_{\mathrm{L1}} \dot{q}_{\mathrm{R1}}\right)^2 dx + \int_{L_2}^{L+L_1} \left(R_{\mathrm{L2}} \dot{q}_{\mathrm{R2}}\right)^2 dx\right) \end{aligned} \tag{21}$$

2.4 Rayleigh dissipation functions

To account for the effect of the mechanical and electrical damping on the system, we define Rayleigh dissipation functions of the PEH as

$$D_{\mathrm{r}} = \frac{1}{2}\mathbf{D}\dot{\mathbf{r}}^{\mathbf{2}}, D_{q_1} = \frac{1}{2} R_{\mathrm{L1}} \dot{q}_{\mathrm{R1}}^2, D_{q_2} = \frac{1}{2} R_{\mathrm{L2}} \dot{q}_{\mathrm{R2}}^2 \tag{22}$$

where D_{r} is the mechanical dissipation function; D_{q1} and D_{q2} are the electrical dissipation functions for SEC1 and SEC2, respectively; and **D** is mechanical damping matrix of the PEH.

2.5 Lagrange's equations

The Lagrange's dynamic equations for the PEH with SEC1 and SEC2 are given by

$$\begin{cases} \dfrac{\mathrm{d}}{\mathrm{d}t}\left(\dfrac{\partial L_{\mathrm{a}}}{\partial \dot{\mathbf{r}}}\right)-\dfrac{\partial L_{\mathrm{a}}}{\partial \mathbf{r}}+\dfrac{\partial D_r}{\partial \dot{\mathbf{r}}}=-\mathbf{B}\ddot{z}_{\mathrm{b}} \\ \dfrac{\mathrm{d}}{\mathrm{d}t}\left(\dfrac{\partial L_{\mathrm{a}}}{\partial \dot{q}_{\mathrm{R1}}}\right)-\dfrac{\partial L_{\mathrm{a}}}{\partial q_{\mathrm{R1}}}+\dfrac{\partial D_{q_1}}{\partial \dot{q}_{\mathrm{R1}}}=0 \\ \dfrac{\mathrm{d}}{\mathrm{d}t}\left(\dfrac{\partial L_{\mathrm{a}}}{\partial \dot{q}_{\mathrm{R2}}}\right)-\dfrac{\partial L_{\mathrm{a}}}{\partial q_{\mathrm{R2}}}+\dfrac{\partial D_{q_2}}{\partial \dot{q}_{\mathrm{R2}}}=0 \end{cases} \tag{23}$$

where Lagrangian $L_{\mathrm{a}}=K-U+W_{\mathrm{e}}=K-(U_{\mathrm{s}}+U_{\mathrm{ps}}-U_{\mathrm{pe}})+(W_{\mathrm{pe1}}+W_{\mathrm{pe2}})$; $\ddot{z}_{\mathrm{b}}$ is the input acceleration; and $\mathbf{B}$ is the effective forcing coefficient vector given by

$$\mathbf{B}=\int_0^L\left(m_{\mathrm{s}}+m_{\mathrm{p}}\right)\boldsymbol{\psi}dx+M_0\boldsymbol{\psi}(L)+S_0\boldsymbol{\psi}'(L) \tag{24}$$

From Eq. (23), the governing equations of the cantilevered PEH with SEC can be obtained as below

$$\begin{cases} \mathbf{M}\ddot{\mathbf{r}}+\mathbf{D}\dot{\mathbf{r}}+\mathbf{K}\mathbf{r}-(\boldsymbol{\Theta}_1 R_{\mathrm{L1}}\dot{q}_{\mathrm{R1}}+\boldsymbol{\Theta}_2 R_{\mathrm{L2}}\dot{q}_{\mathrm{R2}})=-\mathbf{B}\ddot{z}_{\mathrm{b}} \\ \boldsymbol{\Theta}_1{}^{\mathrm{T}}\dot{\mathbf{r}}+C_1^{\mathrm{S}}R_{\mathrm{L1}}\ddot{q}_{\mathrm{R1}}+\dot{q}_{\mathrm{R1}}=0 \\ \boldsymbol{\Theta}_2{}^{\mathrm{T}}\dot{\mathbf{r}}+C_2^{\mathrm{S}}R_{\mathrm{L2}}\ddot{q}_{\mathrm{R2}}+\dot{q}_{\mathrm{R2}}=0 \end{cases} \tag{25}$$

where $\mathbf{M}$ and $\mathbf{K}$ are the mass and stiffness matrices of the PEH, respectively; $\boldsymbol{\Theta}_1$ and $\boldsymbol{\Theta}_2$ are the electromechanical coupling coefficients of the PEH with SEC1 and SEC2, respectively; and C_1^S and C_2^S are the clamped capacitances of the portions of piezoelectric cantilever with SEC1 and SEC2, respectively. Rearranging Eq. (25) by relating the voltage and current, the governing equations of the cantilevered PEH with SEC can be re-written as

$$\begin{cases} \mathbf{M}\ddot{\mathbf{r}}+\mathbf{D}\dot{\mathbf{r}}+\mathbf{K}\mathbf{r}-(\boldsymbol{\Theta}_1 \mathrm{V}_{\mathrm{R1}}+\boldsymbol{\Theta}_2 \mathrm{V}_{\mathrm{R2}})=-\mathbf{B}\ddot{z}_{\mathrm{b}} \\ \boldsymbol{\Theta}_1{}^{\mathrm{T}}\dot{\mathbf{r}}+C_1^{\mathrm{S}}\dot{\mathrm{V}}_{\mathrm{R1}}+\mathrm{V}_{\mathrm{R1}}/R_{\mathrm{L1}}=0 \\ \boldsymbol{\Theta}_2{}^{\mathrm{T}}\dot{\mathbf{r}}+C_2^{\mathrm{S}}\dot{\mathrm{V}}_{\mathrm{R2}}+\mathrm{V}_{\mathrm{R2}}/R_{\mathrm{L2}}=0 \end{cases} \tag{26}$$

In Eq. (26), the entries in the mass, stiffness and damping matrices are given by

$$\begin{aligned} M_{ik}=&\int_0^L(m_{\mathrm{s}}+m_{\mathrm{p}})\psi_i(x)\psi_k(x)dx+M_0\psi_i(L)\psi_k(L) \\ &+S_0\psi_i(L)\psi_k'(L)+S_0\psi_i'(L)\psi_k(L)+I_0\psi_i'(L)\psi_k'(L) \end{aligned} \tag{27}$$

$$\begin{aligned} K_{ik}=&\int_0^L\int_{-h_{\mathrm{s}}/2-h_{\mathrm{p}}}^{-h_{\mathrm{s}}/2}c_{11}^{\mathrm{E}}\hat{z}^2\psi_i''(x)\psi_k''(x)bd\hat{z}dx+\int_0^L\int_{-h_{\mathrm{s}}/2}^{h_{\mathrm{s}}/2}c_{\mathrm{s}}\hat{z}^2\psi_i''(x)\psi_k''(x)bd\hat{z}dx \\ &+\int_0^L\int_{h_{\mathrm{s}}/2}^{h_{\mathrm{s}}/2+h_{\mathrm{p}}}c_{11}^{\mathrm{E}}\hat{z}^2\psi_i''(x)\psi_k''(x)bd\hat{z}dx \end{aligned} \tag{28}$$

$$D_{ik}=\alpha M_{ik}+\beta K_{ik} \tag{29}$$

where α and β are the Rayleigh damping coefficients. They are defined by

$$\zeta_i = \frac{\alpha}{2\omega_i} + \frac{\beta\omega_i}{2} \quad , \quad i=1,2,\ldots,n \tag{30}$$

where ζ_i and ω_i are the damping ratio and the natural frequency of the i-th mode, respectively.

The entries in the effective forcing coefficient vector $\mathbf{B}$ are given by

$$B_i = \int_0^L \left(m_\mathrm{s} + m_\mathrm{p}\right)\psi_i(x)dx + M_0\psi_i(L) + S_0\psi_i'(L) \tag{31}$$

The entries in the electromechanical coupling vectors $\mathbf{\Theta_1}$ and $\mathbf{\Theta_2}$ are given by

$$\begin{cases} \theta_{1\_i} = h_\mathrm{pc} e_{31} b \int_0^{L_1} \psi_i''(x)dx \\ \theta_{2\_i} = h_\mathrm{pc} e_{31} b \int_{L_2}^{L} \psi_i''(x)dx \end{cases} \tag{32}$$

The capacitance terms C_1^S and C_2^S are given by

$$\begin{cases} C_1^S = \dfrac{1}{2h_\mathrm{p}} \int_0^{L_1} \varepsilon_{33}^S b dx = \dfrac{\varepsilon_{33}^S b L_1}{2h_\mathrm{p}} \\ C_2^S = \dfrac{1}{2h_\mathrm{p}} \int_{L_2}^{L+L_\mathrm{t}} \varepsilon_{33}^S b dx = \dfrac{\varepsilon_{33}^S b\left(L + L_\mathrm{t} - L_2\right)}{2h_\mathrm{p}} \end{cases} \tag{33}$$

In order to obtain the expression of steady state voltage responses of $R_{\mathrm{L}1}$ and $R_{\mathrm{L}2}$, Eq. (26) should be decoupled. First, we solve the eigenvector matrix $\mathbf{P}$ of the equation $\mathbf{M\ddot{r}} + \mathbf{Kr} = 0$. Subsequently, substituting $\mathbf{r} = \mathbf{P\eta}$ into Eq. (26) and multiplying the first Eq. (26) by $\mathbf{P^T}$ gives

$$\begin{cases} \mathbf{P^T M P\ddot{\eta}} + \mathbf{P^T D P\dot{\eta}} + \mathbf{P^T K P\eta} - \left(\mathbf{P^T\Theta_1}\mathrm{V}_{\mathrm{R}1} + \mathbf{P^T\Theta_2}\mathrm{V}_{\mathrm{R}2}\right) = -\mathbf{P^T B}\ddot{z}_b \\ \mathbf{\Theta_1}^\mathbf{T}\mathbf{P\dot{\eta}} + C_1^S\dot{\mathrm{V}}_{\mathrm{R}1} + \mathrm{V}_{\mathrm{R}1}/R_{\mathrm{L}1} = 0 \\ \mathbf{\Theta_2}^\mathbf{T}\mathbf{P\dot{\eta}} + C_2^S\dot{\mathrm{V}}_{\mathrm{R}2} + \mathrm{V}_{\mathrm{R}2}/R_{\mathrm{L}2} = 0 \end{cases} \tag{34}$$

Thus, the modal electromechanical coupling governing equations of the PEH with SEC can be written as

$$\begin{cases} \ddot{\eta}_i + 2\zeta_i\omega_i\dot{\eta}_i + \omega_i^2\eta_i - \left(\chi_{1\_i}\mathrm{V}_{\mathrm{R}1} + \chi_{2\_i}\mathrm{V}_{\mathrm{R}2}\right) = -b_i\ddot{z}_\mathrm{b} \\ \sum_{i=1}^{n}\chi_{1\_i}\dot{\eta}_i + C_1^S\dot{\mathrm{V}}_{\mathrm{R}1} + \mathrm{V}_{\mathrm{R}1}/R_{\mathrm{L}1} = 0 \\ \sum_{i=1}^{n}\chi_{2\_i}\dot{\eta}_i + C_2^S\dot{\mathrm{V}}_{\mathrm{R}2} + \mathrm{V}_{\mathrm{R}2}/R_{\mathrm{L}2} = 0 \end{cases} \tag{35}$$

where η_i are the entries in the decoupled displacement vector $\mathbf{\eta}$; b_i are the entries in the decoupled modal force coefficient vector $\mathbf{P^T B}$; χ_{1_i} and χ_{2_i} are the entries in the decoupled modal electromechanical coupling vectors $\mathbf{\Theta_1}^\mathbf{T}\mathbf{P}$ and $\mathbf{\Theta_2}^\mathbf{T}\mathbf{P}$, respectively.

When the harmonic base excitation $\ddot{z}_b = Ae^{j\omega t}$ is applied (where A is the magnitude of base acceleration, j is the unit imaginary number and ω is the excitation frequency), the steady state voltage responses $V_{R1}(t)$ and $V_{R2}(t)$ can be obtained from Eq. (35) as follows,

$$V_{R1}(t)=\frac{\left(\sum_{i=1}^{n}\frac{j\omega\chi_{1\_i}b_i}{\Omega_i^2}\right)\left(\sum_{i=1}^{n}\frac{j\omega\chi_{2\_i}^2}{\Omega_i^2}+j\omega C_2^S+\frac{1}{R_{L2}}\right)-\left(\sum_{i=1}^{n}\frac{j\omega\chi_{2\_i}b_i}{\Omega_i^2}\right)\left(\sum_{i=1}^{n}\frac{j\omega\chi_{1\_i}\chi_{2\_i}}{\Omega_i^2}\right)}{\left(\sum_{i=1}^{n}\frac{j\omega\chi_{1\_i}^2}{\Omega_i^2}+j\omega C_1^S+\frac{1}{R_{L1}}\right)\left(\sum_{i=1}^{n}\frac{j\omega\chi_{2\_i}^2}{\Omega_i^2}+j\omega C_2^S+\frac{1}{R_{L2}}\right)-\left(\sum_{i=1}^{n}\frac{j\omega\chi_{1\_i}\chi_{2\_i}}{\Omega_i^2}\right)^2}A\omega^2e^{j\omega t} \quad (36)$$

$$V_{R2}(t)=\frac{\left(\sum_{i=1}^{n}\frac{j\omega\chi_{2\_i}b_i}{\Omega_i^2}\right)\left(\sum_{i=1}^{n}\frac{j\omega\chi_{1\_i}^2}{\Omega_i^2}+j\omega C_1^S+\frac{1}{R_{L1}}\right)-\left(\sum_{i=1}^{n}\frac{j\omega\chi_{1\_i}b_i}{\Omega_i^2}\right)\left(\sum_{i=1}^{n}\frac{j\omega\chi_{1\_i}\chi_{2\_i}}{\Omega_i^2}\right)}{\left(\sum_{i=1}^{n}\frac{j\omega\chi_{1\_i}^2}{\Omega_i^2}+j\omega C_1^S+\frac{1}{R_{L1}}\right)\left(\sum_{i=1}^{n}\frac{j\omega\chi_{2\_i}^2}{\Omega_i^2}+j\omega C_2^S+\frac{1}{R_{L2}}\right)-\left(\sum_{i=1}^{n}\frac{j\omega\chi_{1\_i}\chi_{2\_i}}{\Omega_i^2}\right)^2}A\omega^2e^{j\omega t} \quad (37)$$

where $\Omega_i^2=\omega_i^2-\omega^2+j2\zeta_i\omega_i\omega$.

In Eq. (36), setting χ_{1_i} and χ_{2_i} to χ_i and zero, respectively, we can obtain the steady state voltage response $V_R(t)$ of the PEH with CEC as follows

$$V_R(t)=\frac{\left(\sum_{i=1}^{n}\frac{j\omega\chi_i b_i}{\Omega_i^2}\right)}{\left(\sum_{i=1}^{n}\frac{j\omega\chi_i^2}{\Omega_i^2}+j\omega C^S+\frac{1}{R_L}\right)}A\omega^2e^{j\omega t} \quad (38)$$

where the decoupled modal electromechanical coupling coefficient is $\chi_i=\chi_{1\_i}+\chi_{2\_i}$ and the static clamped capacitance is $C^S=C_1^S+C_2^S$.

3. Finite element modeling

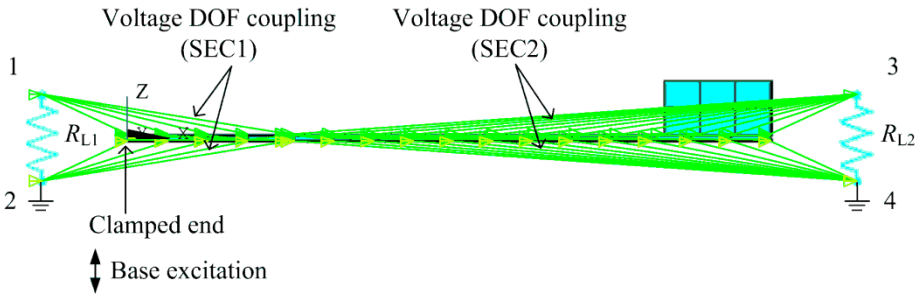

Fig. 2 FE model of PEH with SEC

Finite element method (FEM) provides an alternative way to estimate the performance of the PEH with SEC if simple resistive load is considered. In this section, we use the commercial software ANSYS to establish the FE model of the PEH with SEC, as shown in Fig. 2. The 8-node hexahedral coupled-field element SOLID5 is used for the PZT layer. The 8-node linear structural element SOLID45 is used for the substrate layer. The circuit element CIRCU94 is used to model the resistors.

The piezoelectric coefficients of PZT-5H used in ANSYS are given by Heinonen *et al*. (2005). Since the polarization direction of the piezoelectric material is represented by the sign of the piezoelectric constants, for the symmetric bimorph in series used in this paper, the signs of the piezoelectric constants for the top and bottom piezoelectric plates are opposite. In addition, the electrode layer can be simulated by coupling the nodal voltage degrees of freedom (DOF) to ensure a uniform electrical potential. For SEC1, the voltage DOFs on the upper and bottom electrode surfaces are coupled to common nodes "1" and "2", respectively, as shown in Fig. 2. These common nodes "1" and "2" are connected to the resistor R_{L1}. Similar procedure is applied for SEC2. Common nodes "2" and "4" are defined as ground. It should be mentioned that Fig. 2 is just an illustration on how to model a PEH in ANSYS. In the later part of this article, the mesh of the FE model is further refined.

4. Equivalent circuit modeling

The above theoretical model and FE model can account for pure resistive load, i.e., they can predict the maximal achievable power from each segmented electrode configuration. Once the two electrical ports are intended to deliver the power to a common load, a sophisticated interface circuit including multiple rectifiers is required. In such case, theoretical modeling becomes cumbersome or even impossible. The ECM of the proposed PEH with SEC is presented in this section to address this issue.

Table 1 Analogy between mechanical and electrical domains

Mechanical parameters at *i*-th mode	Equivalent circuit parameters at *i*-th mode
Modal coordinate: $\eta_i(t)$	Charge: $q_i(t)$
Modal velocity: $d\eta_i(t)/dt$	Current: $i_i(t)$
1	Inductance: L_i
$2\zeta_i\omega_i$	Resistance: R_i
$1/\omega_i^2$	Capacitance: C_i
Modal force: $-b_i\ddot{z}_b$	Voltage source: $v_i(t)$
Electromechanical coupling: $-\chi_i$, $-\chi_{1\_i}$, $-\chi_{2\_i}$	Turn ratio of ideal transformer: N_i, N_{1_i}, N_{2_i}

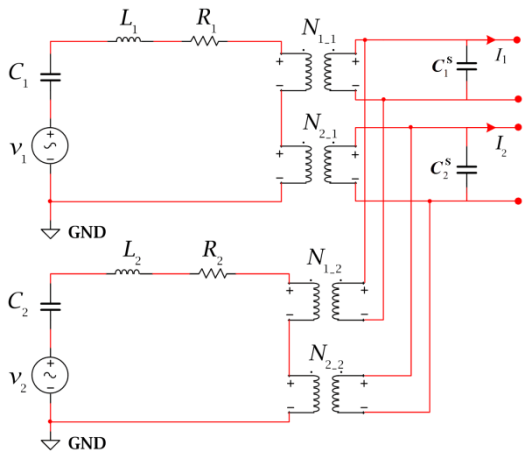

Fig. 3 Multi-mode ECM of cantilevered PEH with SEC1 and SEC2

The electromechanical governing equation of the piezoelectric coupling system (Eq. (35)) can be written as the governing equation of a circuit network if we apply the analogy between the mechanical and electrical domains, as shown in Table 1. Based on the governing equation derived by theoretical analysis, we can determine the equivalent circuit parameters of the PEH with SEC through the analogy. Since our study focuses on the maximal power output achievable from the first two vibration modes, the electrode of the PEH with SEC is segmented at the strain node of the second bending mode. The electromechanical coupling coefficients of SEC1 and SEC2 can be analogized as two separate ideal transformers at the same vibration mode. Here, we construct two branches circuit network accounting for the first two modes, each composed of an inductor, a capacitor, a resistor, an ideal voltage source, and two ideal transformers as shown in Fig. 3.

5. Model validation

In this section, the ECM of the cantilevered PEH with SEC is validated using the theoretical analysis and FEA. For model validation, we consider two pure resistive loads attached to two electrical output ports of the PEH with SEC such that the theoretical analysis, the FEA and the ECM-based method are all applicable to estimate the outputs. The material and geometric parameters of the cantilevered PEH are listed in Table 2, where the reduced piezoelectric constants (C_{11}^{E}, e_{31} and $\varepsilon_{33}^{\mathrm{S}}$) for the Euler–Bernoulli theory are calculated according to du Toit (2005). Based on theoretical analysis, the normalized strain of the piezoelectric cantilever with a proof mass are plotted for the first two modes, as shown in Fig. 4. It can be seen from Fig. 4 that a strain node appears at x=0.3L for the second mode.

According to the analogy between the mechanical and electrical domains as listed in Table 1, we obtain equivalent circuit parameters in the ECM of the PEH with SEC, as listed in Table 3. Fig. 5 shows the multi-mode ECM for the proposed PEH with resistive loads. It should be noted that the parameters from the theoretical analysis such as the ideal voltage sources and the transformer ratios may be positive or negative. However, the SPICE software only accepts positive input

values. We can avoid this problem by changing the wire connection pattern. For example, at the first mode, voltage source v_1 is negative. Thus, the terminals of v_1 are swapped, as shown in Fig. 5. At the second mode, the transformer ratios N_{2_2} and voltage source v_2 are negative. Thus, the terminals of both N_{2_2} and v_2 are swapped. In addition, since two transformers (N_{1_1} and N_{1_2}) represent the coupling of SEC1 at two modes, their output terminals should be connected to the clamped capacitance C_1^S from SEC1. Similarly, the output terminals of N_{2_1} and N_{2_2} should be connected to the clamped capacitance C_2^S from SEC2.

Table 2 Material and geometric properties of cantilevered PEH with SEC

Item	Value
Density of piezoelectric layer, ρ_p (kg/m^3)	7500
Density of substrate layer, ρ_s (kg/m^3)	8920
Stiffness of piezoelectric layer, C_{11}^E (GPa)	60.6
Stiffness of substrate layer, c_s (GPa)	113
Piezoelectric constant, e_{31} (C/m^2)	-16.6
Permittivity of piezoelectric layer, ε_{33}^S (nF/m)	21
Length of total beam, $L+L_t$ (mm)	60
Length of active beam, L (mm)	50
Length of proof mass, L_t (mm)	10
Length of SEC1, L_1 (mm)	15
Length of SEC2, $L+L_t-L_2$ (mm)	44.5
Width of beam and proof mass, b (mm)	20
Thickness of piezoelectric layer, h_p (mm)	0.2
Thickness of substrate layer, h_s (mm)	0.3
Thickness of proof mass, h_t (mm)	5
Damping ratio at the first mode, ζ_1	0.048
Damping ratio at the second mode, ζ_2	0.026

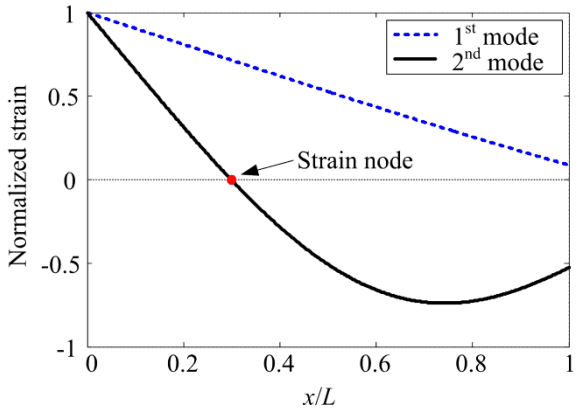

Fig. 4 Normalized strain distribution of cantilevered PEH for the first two bending modes

Table 3 Parameters of ECM of PEH with SEC determined from theoretical analysis

i-th mode	L_i	R_i	C_{2_i}	N_{1_i}	N_{2_i}	v_i	C_1^S	C_2^S
1	1	22.2195	1.64E-5	0.0102	0.0106	-1.1015	1.5753E-8	4.6735E-8
2	1	136.86	1.44E-7	0.0663	-0.1671	-0.3854		

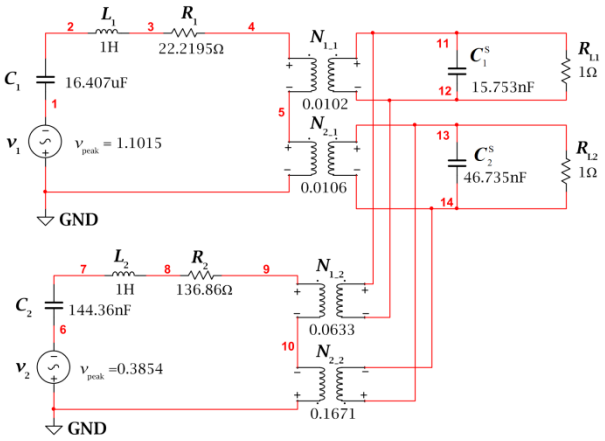

Fig. 5 Multi-mode ECM of cantilevered PEH with SEC1 and SEC2 attached with resistive loads

Figs. 6 and 7 compare the magnitude and phase of the short circuit current of the PEH with SEC from the ECM, theoretical analysis and FEA, respectively. Because the short circuit current can be predicted using low values of load resistances ($R_{L1}\rightarrow 0$ and $R_{L2}\rightarrow 0$), two resistors of 1Ω are used to estimate the short circuit current of SEC1 and SEC2. It can be seen from Figs. 6 and 7 that the results of the ECM agree perfectly with those from the analytical model and FEA. It should be mentioned that in Fig. 7, SEC1 and SEC2 are in-phase at the first mode; however, they are out-of-phase at the second mode. Hence, the SEC is needed for the energy harvesting in the higher vibration mode to avoid the electrical cancellation caused by the CEC.

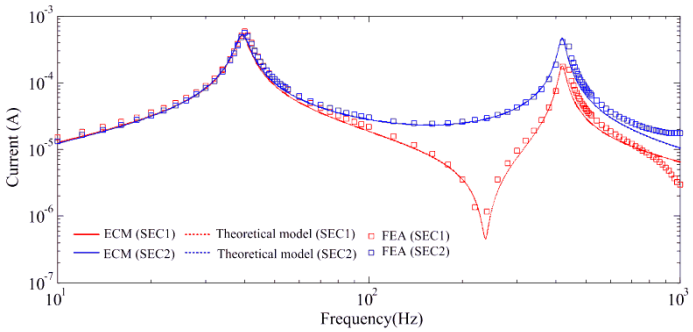

Fig. 6 Magnitude of short circuit current (R_{L1}= R_{L2}=1Ω) under excitation of 9.8 m/s^2

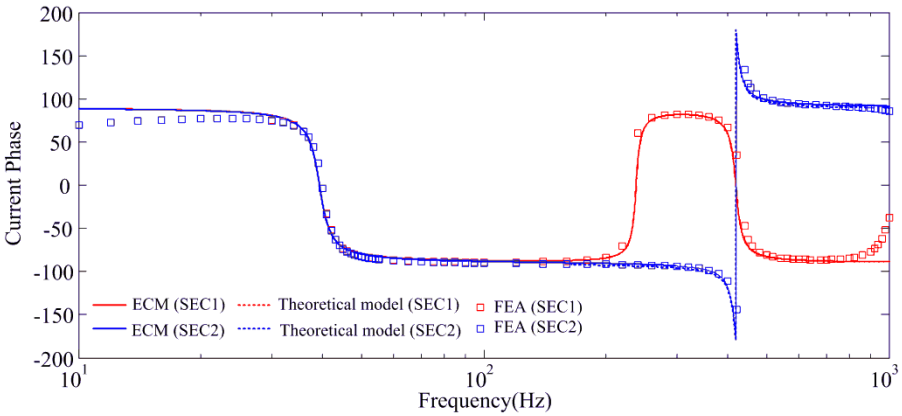

Fig. 7 Phase of short circuit current (R_{L1}= R_{L2}=1Ω) under excitation of 9.8 m/s^2

Figs. 8 and 9 compare the magnitude and phase of the open circuit voltage of the PEH with SEC from the ECM, theoretical model and FEA, respectively. Because the open circuit voltage can be predicted using large values of load resistances ($R_{L1}\rightarrow\infty$ and $R_{L2}\rightarrow\infty$), two resistors of 1MΩ are used to estimate the open circuit voltage of SEC1 and SEC2. Again, the results obtained from the ECM are very close to those from theoretical model and FEA, as shown Figs. 8 and 9. It should be mentioned that in Fig. 9, the phase is plotted between -180° and +180°. In the frequency range of 100 Hz~400 Hz, the phase angle is very close to -180° or +180°. Although the theoretical model, FEA and ECM-based method show a discrepancy at the location where the phase is switched from -180° to +180°, this does not undermine the validity of the phase estimation since phase angles of -180° and +180° actually refer to the same. Therefore, the above results validate the derived ECM for performance evaluation of the PEH with SEC.

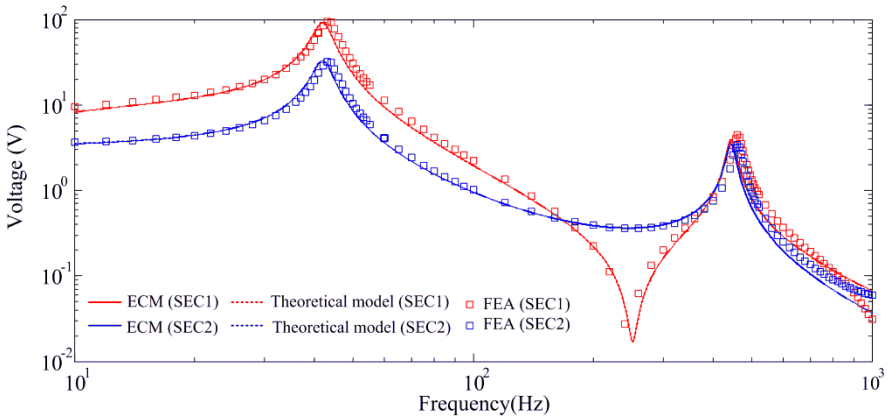

Fig. 8 Magnitude of open circuit voltage (R_{L1}= R_{L2}=1MΩ) under excitation of 9.8 m/s^2

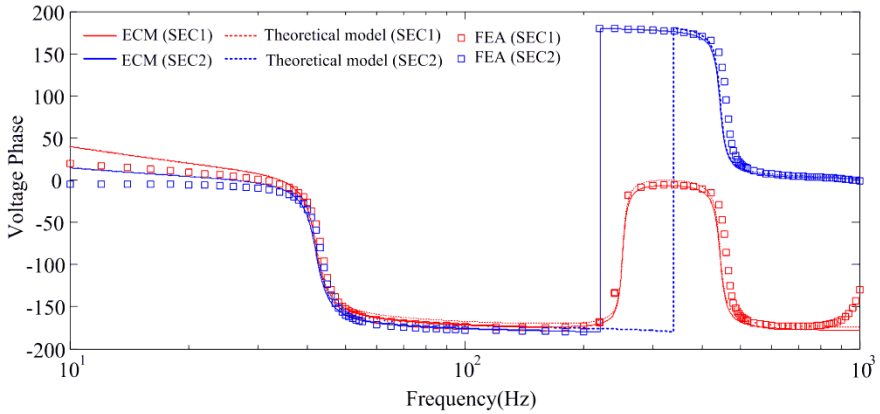

Fig. 9 Phase of open circuit voltage (R_{L1}= R_{L2}=1MΩ) under excitation of 9.8 m/s^2

6. Improved performance with SEC

With the validated ECM, in this section, the optimal power outputs with SEC and CEC are compared, considering practical DC interface circuits. Figs. 10 and 11 show the interface circuits for cantilevered PEH with SEC and CEC, respectively. In Fig. 10, two electrical ports are connected to two separate rectifiers to avoid the electrical cancellation, and then deliver power to a common load. Here, the two rectifiers are connected in parallel.

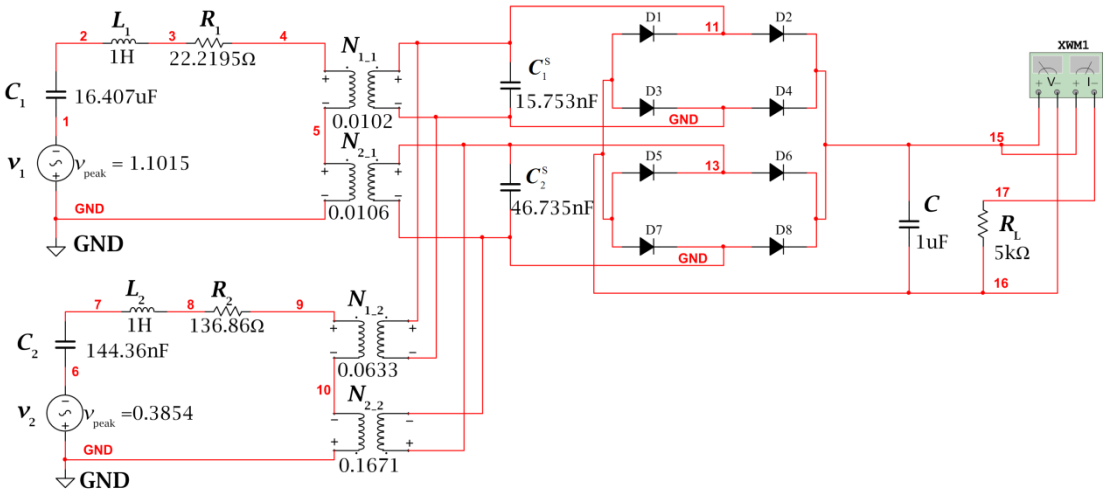

Fig. 10 System diagram of cantilevered PEH with SEC

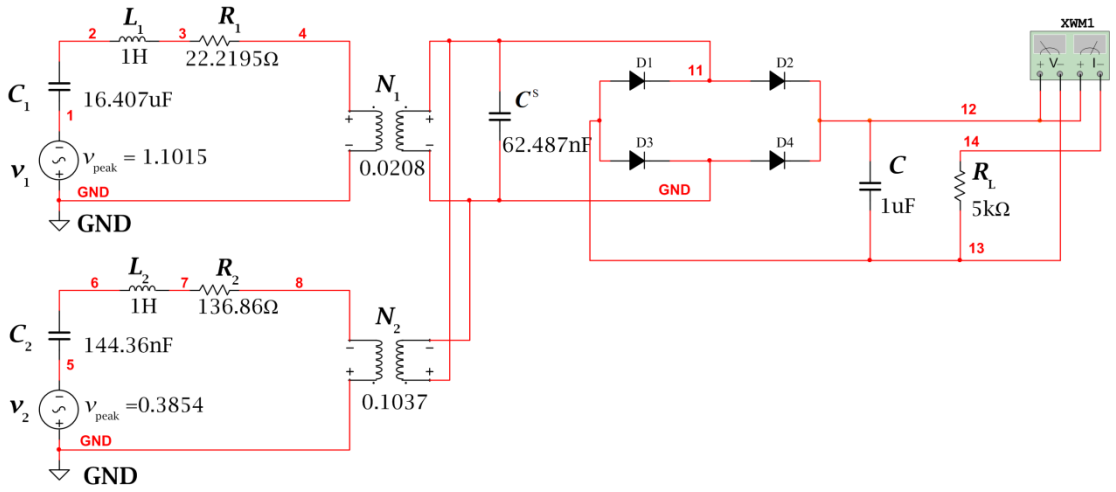

Fig. 11 System diagram of cantilevered PEH with CEC

Table 4 lists the power outputs of the PEH with SEC for various load resistances at different excitation frequencies. It should be mentioned that Table 4 illustrates how to determine the optimal power from the PEH. For example, for frequency at 40 Hz, by changing the load resistance, the optimal power is determined as 5.514 mW at 80kΩ. Similarly, the optimal power for frequency 40.2 Hz is determined as 5.573 mW when the load resistance is 100kΩ. Following the procedure in the table, the optimal power outputs at other frequencies can be determined and plotted in Fig. 12. Fig. 12 compares the optimal power outputs from the PEH with SEC and CEC at the first two vibration modes. It is observed that the performance with SEC has no substantial difference from that with CEC at the first mode. However, SEC improves power magnitude by two times and enlarges the bandwidth (the frequency range between two half power points) by about 80% as compared to those of CEC near the second mode, as shown in Fig. 12(b).

Table 4 Power outputs of PEH with SEC for various load resistances and excitation frequency under excitation of 9.8 m/s^2

R_L(kΩ) / Freq (Hz)	60	80	100	120	140	160	…
40	5.431mW	5.514mW	5.491mW	5.402mW	5.275mW	5.155mW	
40.2	5.497mW	5.548mW	5.573mW	5.520mW	5.420mW	5.319mW	
40.5	5.229mW	5.469mW	5.565mW	5.568mW	5.517mW	5.541mW	
41	4.688mW	5.034mW	5.224mW	5.309mW	5.332mW	5.325mW	
…							

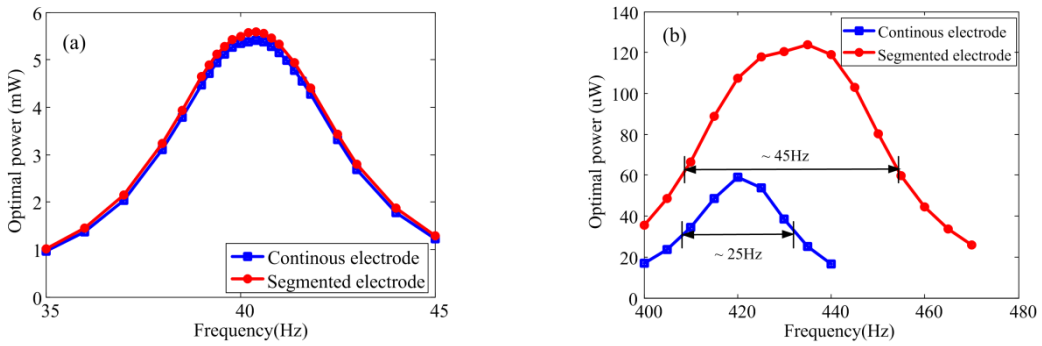

Fig. 12 Comparison of optimal power outputs with SEC and CEC at (a) 1st mode and (b) 2nd mode under excitation of 9.8 m/s^2

7. Conclusions

In this paper, a mathematical model of the PEH with SEC is developed by simplifying the energy harvesting interface circuit as pure resistors. It can be used to estimate the power from each segmented electrode pair. However, the theoretical analysis is difficult to achieve when a practical DC interface circuit is considered, i.e., the output of each electrode pair of SEC is separately rectified and delivered to a common load to avoid the electrical cancellation at a higher vibration mode. In such case, a method based on equivalent circuit modeling and circuit simulation is proposed to address this challenge. The parameters in the ECM considering multiple modes are identified by the theoretical analysis. The ECM with multiple rectifiers is then established and simulated in the SPICE software. With the proposed ECM-based modeling method, we can provide a comprehensive evaluation of the performance with SEC, which is not available in the literature. We also demonstrated the advantageous performance of the cantilevered PEH with SEC over that with CEC, in terms of two times larger magnitude of output power and 80% increase in bandwidth near the second mode.

Acknowledgments

The research described in this paper was financially supported by the Natural Science Foundation of China (No.51077018) and Heilongjiang Provincial Natural Science Fund (F201219) and the Program for Young Teachers Scientific Research in Qiqihar University (2012k-Z12).

References

Aladwani, A., Arafa M., Aldraihem, O., Baz, A. (2012), "Cantilevered piezoelectric energy harvester with a dynamic magnifier", *J.Vib. Acoust.*, **134**(3), 031004.

Anton, S.R. and Sodano, H.A. (2007), "A review of power harvesting using piezoelectric materials (2003-2006)", *Smart Mater. Struct.,* **16**(3), 1-21.
Beeby, S.P., Tudor, M.J. and White, N.M. (2006), "Energy harvesting vibration sources for microsystems applications", *Meas. Sci. and Technol.*, **17**(12), 175- 195.
du Toit, N. (2005), *Modeling and design of a MEMS piezoelectric vibration energy harvester*, MS Thesis, Massachusetts Institute of Technology, Boston.
du Toit, N., Wardle, B.L. and Kim, S.G. (2005), "Design considerations for MEMS-scale piezoelectric mechanical vibration energy harvesters", *Integr. Ferroelectr.*, **71**,121-160.
Erturk, A. and Inman, D.J. (2008), "A distributed parameter electromechanical model for cantilevered piezoelectric energy harvesters", *J.Vib. Acoust.*, **130**(4), 041002.
Erturk, A., Tarazaga, P.A., Farmer, J.R. and Inman, D.J. (2009), "Effect of strain nodes and electrode configuration on piezoelectric energy harvesting from cantilevered Beams", *J.Vib. Acoust.*, **131**(1), 0110101-01101011.
Elvin, N.G. and Elvin, A.A. (2009), "A general equivalent circuit model for piezoelectric generators", *J. Intel. Mat. Syst. Str*., **20**(1), 3-9.
Foisal, A.R., Hong, M.C. and Chung, G.S. (2012), "Multi-frequency electromagnetic energy harvester using a magnetic spring cantilever", *Sensor. Actuat. A - Phys.*, **182**, 106-113.
Guan, X.C., Huang, Y.H., Li, H. and Ou, J.P. (2012), "Adaptive MR damper cable control system based on piezoelectric power harvesting", *Smart Struct. Syst*., **10**(1), 33-46.
Guyomar, D., Badel, A., Lefeuvre, E. and Richard, C. (2005), "Toward energy harvesting using active materials and conversion improvement by nonlinear processing", *IEEE T. Ultrason. Ferr.*., **52**(4), 584-595.
Hagood, N.W., Chung, W. and Von, Flotow A. (1990), "Modelling of piezoelectric actuator dynamics for active structural control", *J. Intel. Mat. Syst.Str*., **1**(3), 327-354.
Heinonen, E., Juuti, J. and Leppavuori, S. (2005), "Characterization and modelling of 3D piezoelectric ceramic structures with ATILA software", *J. Eur. Ceram. Soc*., **25**(12), 2467-2470.
Jung, H.J., Kim, I.H. and Koo, J.H. (2011), "A multi-functional cable-damper system for vibration mitigation, tension estimation and energy harvesting", *Smart Struct. Syst*., **7**(5), 379-392.
Kim, M., Hoegen, M., Dugundji, J. and Wardle, B.L. (2010), "Modeling and experimental verification of proof mass effects on vibration energy harvester performance", *Smart Mater. Struct*., **19**(4), 045023.
Kim, S., Clark, W.W. and Wang, Q.M. (2005), "Piezoelectric energy harvesting with a clamped circular plate: analysis", *J.Intel. Mat. Syst. Str*., **16**(10), 847-854.
Lallart, M., Pruvost S. and Guyomar, D. (2011), "Electrostatic energy harvesting enhancement using variable equivalent permittivity", *Phys. Lett. A.*, **375**(45), 3921-3924.
Liang, J.R. and Liao,W.H. (2012), "Impedance modeling and analysis for piezoelectric energy harvesting systems", *IEEE-ASME Trans.Mechatron*., **17**(6),1145-1157.
Liang, J.R. and Liao,W.H. (2012), "Improved design and analysis of self-powered synchronized switch interface circuit for piezoelectric energy harvesting systems", *IEEE T. Ind. Electron*., **59**(4), 1950-1960.
Lien, I.C. and Shu, Y.C. (2011), "Array of piezoelectric energy harvesters", *Proceedings of the SPIE, Conference on Active and Passive Smart Structures and Integrated Systems*, San Diego, March.
Lien, I.C., Shu, Y.C., Wu, W.J., Shiu, S.M. and Lin, H.C. (2010), "Revisit of series-SSHI with comparisons to other interfacing circuits in piezoelectric energy harvesting", *Smart Mater. Struct*., **19** (12), 125009.
Liu H.C., Tay C.J., Quan C.G., Kobayashi T. and Lee C.K. (2011), "Piezoelectric MEMS energy harvester for low-frequency vibrations with wideband operation range and steadily increased output power". *J. Microelectromech. S.*, **20**(5), 1131-1142.
Mathuna, C.O., O'Donnell, T., Martinez-Catala, R.V., Rohan, J. and O'Flynn, B. (2008), "Energy scavenging for long-term deployable wireless sensor networks", *Talanta*, **75**(3), 613-623.
Paradiso, J.A. and Starner T. (2005), "Energy scavenging for mobile and wireless electronics", *IEEE Pervasive Comput.*, **4**(1), 18-27.
Roundy, S., Wright, P.K. and Rabaey, J. (2003), "A study of low level vibrations as a power source for wireless sensor nodes", *Comput. Commun.,* **26**(11), 1131-1144.

Sodano, H.A., Park, G. and Inman, D.J. (2004), "Estimation of electric charge output for piezoelectric energy harvesting", *Strain*, **40**(2), 49-58.
Tang, L.H. and Yang, Y.W. (2011), "Analysis of synchronized charge extraction for piezoelectric energy harvesting", *Smart Mater. Struct*., **20**(8), 085022.
Tang, L.H. and Yang, Y.W. (2012), "A multiple-degree-of-freedom piezoelectric energy harvesting model", *J. Intel. Mat. Syst. Str*., **23**(14), 1631-1647.
Tang, G., Liu J.Q., Yang, B., Luo, J.B., Liu, H.S., Li, YG, Yang, C.S., He DN, Dao VD, Tanaka K and Sugiyama S (2012), "Fabrication and analysis of high-performance piezoelectric MEMS generators", *J. Micromech. Microeng*., **22**(6), 065017.
Wang, H.Y., Shan, X.B. and Xie, T. (2012), "An energy harvester combining a piezoelectric cantilever and a single degree of freedom elastic system", *J. Zhejiang Univ. Sci. A*, **13**(7), 526-537.
Wu, H., Tang, L.H., Yang, Y.W. and Soh, C.K. (2013), "A novel two-degrees-of-freedom piezoelectric energy harvester", *J. Intel. Mat. Syst. Str*., **24**(3), 357-368.
Yang, Y.W. and Tang, L.H. (2009), "Equivalent circuit modeling of piezoelectric energy harvesters", *J. Intel. Mat. Syst. Str*., **20**(18), 2223-2235.
Yang, Y.W., Tang, L.H. and Li H.Y. (2009), "Vibration energy harvesting using macro-fiber composites", *Smart Mater. Struct*., **18**(11), 115025.
Zhang, Y. and Zhu, B.H.,(2012), "Analysis and simulation of multi-mode piezoelectric energy harvesters", *Smart Struct. Syst*., **9**(6), 549-563.

CC